J. of Thermal Science Vol.9, No.3

Numerical Study of Spray Dispersion in a Premixing Chamber for Low-NOx Engines

Jorge Barata **André Silva**
Universidade da Beira Interior, Aerospace Sciences Department, Rua Marquês d'Ávila e Bolama, 6200 Covilhã, Portugal

The present work describes a numerical study of a confined two-phase flow under high-pressure conditions, typical of gas turbine combustors.
An Eulerian frame was used for the gas phase together with a Lagrangian approach to describe the dispersed phase.
The computational method was extended to high-pressure environments, which are more representative of the practical gas turbine operating conditions.
The results are compared with experimental data, and revealed the ability of the model to increase the knowledge of the turbulent dispersion phenomena for this type of practical conditions (high pressure and confined flow).

Keywords: two-phase flows, sprays, high pressure.

Introduction

The present work is devoted to particle dispersion in confined two-phase turbulent jets, which has become a major domain of research attracting increasingly interest and with challenging fundamental aspects. Describing the motion of a dispersed phase is complex and is of great interest in several practical systems. The applications that require the solution of this problem are as varied as the dispersion of passive pollutant particles in the atmosphere to combustion systems with dispersing fuel particles. At present, considerable effort is being made to lower the emissions of oxides of nitrogen (NOx) and other minor species from aircraft gas turbine engines. However, advanced technology for significantly lowering NOx emissions has not been incorporated into current production engines, and more research in particle dispersion is needed to improve gas turbine design methods.

A comprehensive understanding of the spray dispersion process requires a detailed knowledge of the interaction mechanism between the droplets and the surrounding turbulent fluid. Earlier theoretical and experimental investigations of two-phase jets have recently been reviewed[1,2], and in general they have shown a strong influence of operating parameters such as size distribution, mass loading and droplet/gas aerodynamics.

The present work follows that for unconfined and atmospheric conditions of Barata and Perestrelo[2] and Heitor and Moreira[3], which have addressed the question of the lack of available data on polydisperse two-phase turbulent jets, and anisotropy effects.

Received 2000

Here, the numerical work of Barata and Perestrelo[2] is extended to confined and high pressure conditions, and aims to contribute to a better knowledge of the phenomena occurring inside the premix-prevaporize duct of Low-NOx engines, based on measurements of Barros[4]. The flow configuration is shown in Figure 1 and consists in a carrier duct flow air, in range between 3.0 and 6.0 bar. The spray is injected horizontally at the centre of the pipe with a mass flow rate of water of 14.4 kg/h using a commercial 45° full-cone pressure atomiser, DELAVAN WDB 2.25-45. The droplets distribution follow closely a normal size distribution with a number-average particle diameter of 60μm and a standard deviation of 17μm. The air flow is unswirled and the mass flow rate of air varied between 535 kg/h and 752 kg/h, as summarised in Table 1.

The next section gives the details of the computational model. Section III presents a quantitative comparison of numerical results with measurements of Barros[4]. The final section summarises the main findings and conclusions of this work.

Computational Model

The numerical results presented are based on an Eulerian/Lagrangian approach described in detail by Barata and Perestrelo[2], and only the main features are summarised here.

The dispersed phase was treated using a Lagrangian reference frame. This is the most natural form to treating this phase, being assumed that the particles are sufficiently dispersed so that particle-particle interaction is negligible. It is also assumed that the mean flow is steady and material properties of the phases are constant.

Nomenclature

D	=	Diameter of the jet
D_p	=	Particle diameter
g	=	Gravitational acceleration
k	=	Turbulent kinetic energy
m	=	Mass flow rate
p	=	Pressure
R	=	Radial co-ordinate
R_e	=	Reynolds number
U	=	Axial velocity, $u = U + u'$
V	=	Radial velocity, $v = V + v'$
X	=	Axial co-ordinate

Greek symbols

ε	=	Dissipation rate of turbulent kinetic energy
μ	=	Dynamic viscosity
ν	=	Kinematic viscosity
ρ	=	Density

Subscripts

0	=	jet-exit conditions
F	=	Fluid property
P	=	Particle property

Table 1 Summary of test conditions

RUN	p_{air} (bar)	Q_{air} (m^3/h)	m_{air} (kg/h)	U_{air} (m/s)	Re (10^5)	P_{water} (bar)	Δp (bar)	m_{water} (kg/h)
1	3	153	752	6.4	1.23	16	13	14.4
2	3	110	535	4.6	0.88	16	13	14.4
3	6	90	752	3.8	1.46	19	13	14.4

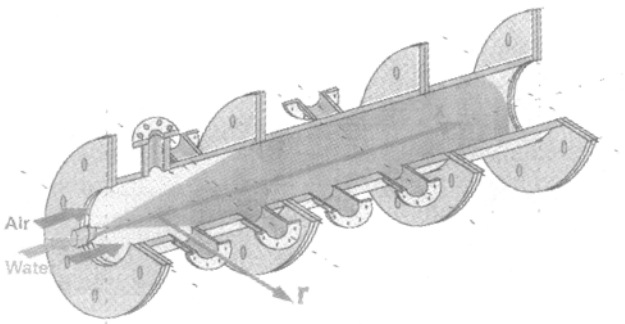

Fig.1 Flow configuration

Particle trajectories were obtained by solving the particle momentum equation through the Eulerian fluid velocity field, for 20 groups of 2,000 particles that were found to be statistically representative of the measured distribution.

The equations used to calculate the position and velocity of each particle were obtained considering the usual simplification for dilute particle-laden flows[6, 7]. Static pressure gradients are small, particles can be assumed spherical and particle collisions can be neglected. Since $\left(\frac{\rho_p}{\rho_f} > 200\right)$, the effects of Basset, virtual mass, Magnus, Saffman and buoyancy forces are negligible[6, 7].

The sizes of the particles are generated randomly so that their distribution corresponds to the experimental data.

The initial position at the injector exit is also generated randomly and the initial velocity and turbulent kinetic energy are obtained from the measurements for the corresponding location. Using the particle equation the next particle velocity is obtained. The new position of particle is calculated by integrating the velocity equation of particle over the time step given by the minimum of the local eddy transit time and the local eddy lifetime. The corresponding particle source terms are stored, and the process is repeated until the particle leaves the calculation domain.

The fluctuating velocity components are generated and added to the local velocity components. Anisotropic effects were take into account by using two fluctuating velocities u_1' and u_2' sampled independently, that were
correlated using the correlation coefficient R_{uv}:

$$u_f' = u_1'$$

$$v_f' = R_{uv}u_1' + \sqrt{1 - R_{uv}^2}u_2'$$

where $R_{uv} = \dfrac{\overline{u'v'}}{\sqrt{\overline{u_f'^2}}\sqrt{\overline{v_f'^2}}}$ was obtained from the measurements.

The gaseous or continuous phase was treated using an Eulerian model based on solution of conservation equations for momentum and mass. Turbulence is modelled with "k-ε" turbulence model. The solution procedure for the continuous phase is based on the SIMPLE algorithm[9] widely used and reported in the literature.

The interaction between the continuous and dispersed phase is introduced by treating particles as sources of mass, momentum and energy to the gaseous phase[8]. A solution for the gaseous field assuming no particle trajectories and source terms is calculated. The gas field is then recomputed with the contribution of the particle source terms. This process is repeated until convergence is achieved.

The computational domain has four boundaries where dependent variables are specified: an inlet and

outlet radius, a symmetry axis and a wall parallel to the axis. The sensivity of the solutions to the location of boundaries was investigated, and their final position is sufficiently far away from injector so that the influence on the computed results is negligible. At the inlet a velocity profile obtained from measurements was used for the axial velocity. On the symmetry, the normal velocity vanishes, and the normal derivatives of the other variables are zero. At the outflow boundary, the gradients of dependent variables in the axial direction are set to zero. At the wall, the wall function method described in detail by Launder and Spalding[5] is used to prescribe the boundary conditions for the velocity and turbulence quantities, assuming that the turbulence is in the state of local equilibrium.

Results and Discussion

In this section, the numerical predictions are compared with the measurements of Barros[4] in a duct of high pressure. The test section was formed by a horizontal cylindrical duct with an inner diameter of 92 mm and a length of 0.5 meters.

The predictions of the velocity field and mean axial velocity profiles of the gaseous phase are used to test the grid independence of the results. Figure 2 compares non-dimensional profiles of mean axial velocity for the different sizes of grids at X/D = 0.7, X/D = 1.7 and X/D = 3.2, and show that the results are already independent of numerical influences for 31x31 grids.

The influence of particles in properties of transport phase is now discussed with the help of Figure 3. The figure shows for the chosen grid of 43x43 points, the velocity field of gas without particles (Fig. 3a) and with particles (Fig. 3b) in the region near the injector. The gaseous flow is accelerated along centreline revealing that the gaseous phase is strongly affected by the presence of particles. In spite of the conical shape of the spray and the initial oblique trajectories of the droplets, the gaseous flow is essentially parallel to the axis of symmetry and no significant radial velocity components can be observed. This result is probably associated with the large velocity of the droplets near the injector that corresponds to very small transit times. As a consequence, the droplets cross the turbulent eddies without much interaction, because of the lack of time, and the contribution to the source term in the momentum equation is quite small.

Figures 4 to 7 show non-dimensional radial profiles of the mean axial velocity and the mean radial velocity.

The radial profiles of mean axial velocity (Figs. 4 and 5) reveal that the exchange of momentum and turbulence energy between two phases is very important for this type of flow configuration. Figures 4 and 5, at X/D = 0.7 and X/D = 1.7, show an acceleration of the gas due to the presence of particles in the central line, at Y/D = 0. The results of Figs. 4 and 5 also show that the drift velocity among two-phases is large for X/D = 0.7, and follow reasonably well the experimental results.

The radial profiles of the mean axial velocity revealed that the smaller particles follow the gaseous flow, while the larger move faster initially (at X/D = 0.7) and then are retarded by the gas until they reach its velocity at X/D = 3.2.

The radial component of the velocity increases with the distance to the symmetric axis of the duct at X/D = 0.7 (Figs. 6 and 7), revealing the use of the constant axial component at the injector exit. For $X/D \geq 1.7$ the radial component of the velocity is practically null as expected due to the confinement of the flow.

The profiles of the component velocity V show that the smallest drops possess the smaller radial velocity component. Consequently they are concentrated on the axis of the duct, and due to its inertia, they reach more distant places on the symmetry axis of the duct.

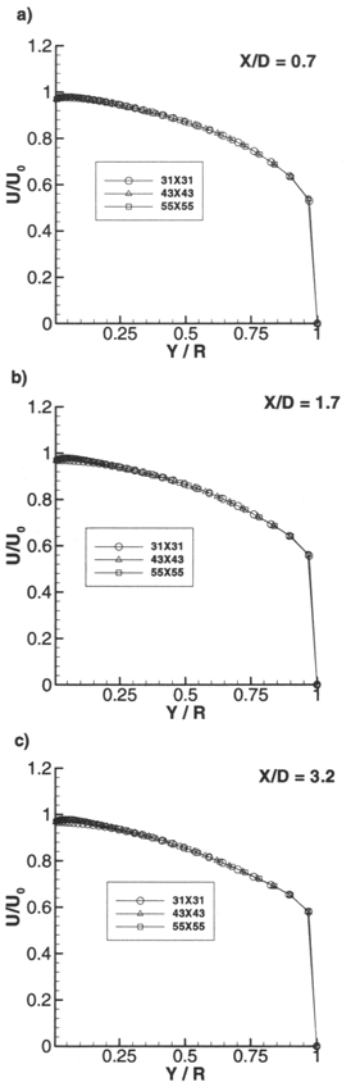

Fig.2 Non-dimensional profiles of the mean axial velocity

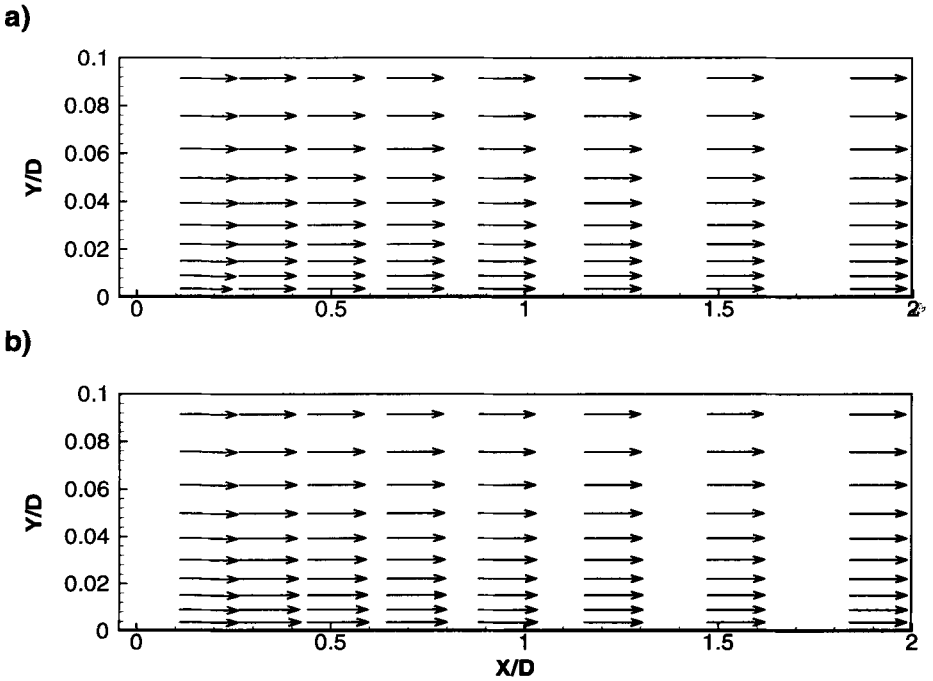

Fig.3 Velocity field of the gas for 3 bar and m_{air} = 752 kg/h: a) without particles; b) with particles

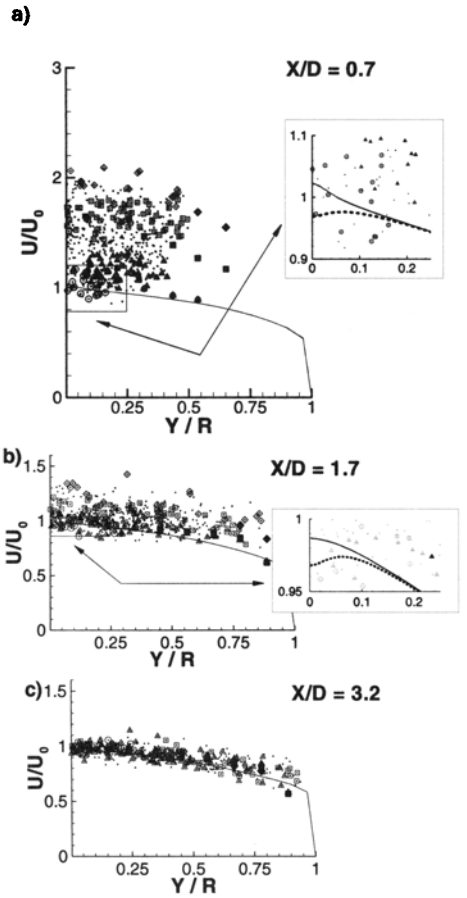

Fig.4 Radial velocity profiles of the mean axial velocity, U, for p_{air}= 3bar and m_{air}= 752 kg/h. Gaseous phase: — with droplets, ------ pure gas (without droplets). Particles: Expts. ● 10-20μm; ▲ 40-50μm; ■ 70-80μm; ◆ 100-110μm; predictions: O <30μm; Δ 40-50μm; □ 70-80μm; ◊ >90μm

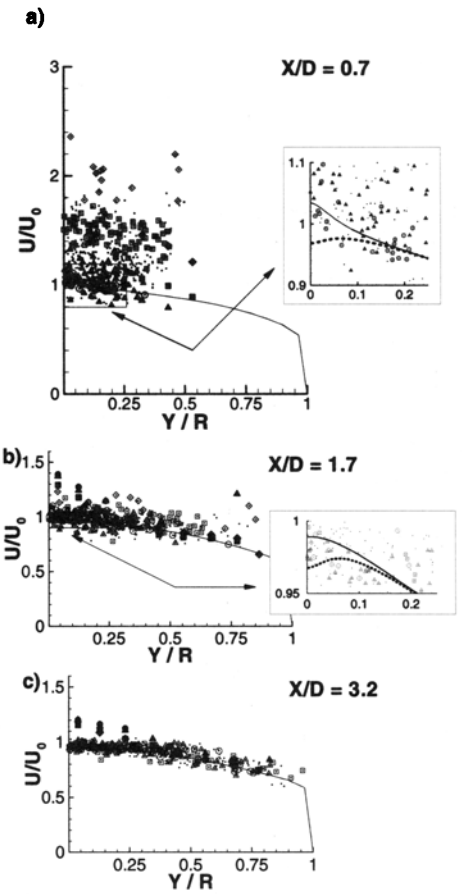

Fig.5 Radial velocity profiles of the mean axial velocity, U, for p_{air}= 6bar and m_{air}= 752 kg/h . Gaseous phase: — with droplets, ----- pure gas (without droplets). Particles: Expts. ● 10-20μm; ▲ 40-50μm; ■ 70-80μm; ◆ 100-110μm; predictions: O <30μm; Δ 40-50μm; □ 70-80μm; ◊ >90μm

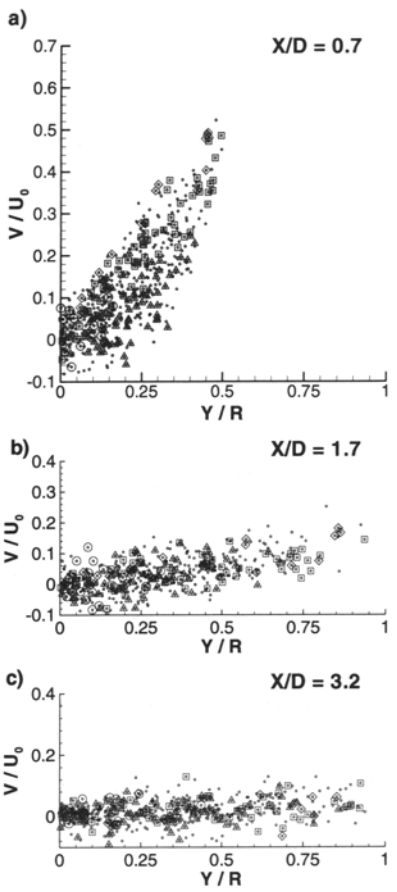

Fig.6 Radial velocity profiles of the mean radial velocity, V, for p_{air}= 3bar and m_{air}= 752 kg/h . Particles: predictions: O <30μm; Δ 40-50μm; □ 70-80μm; ◊ >90μm

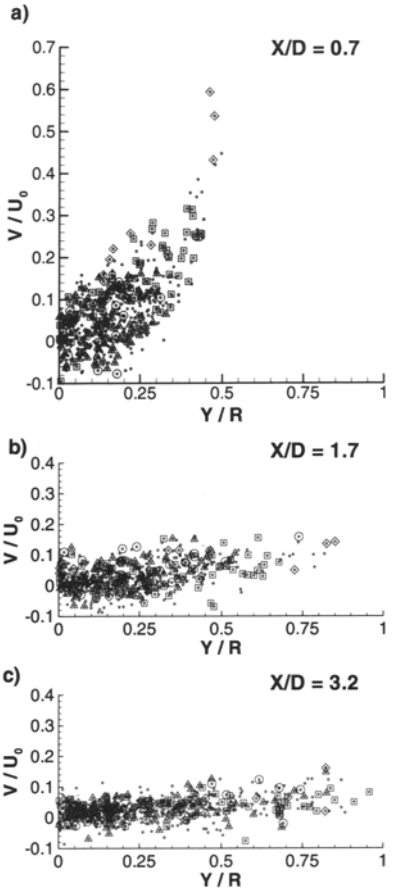

Fig.7 Radial velocity profiles of the mean radial velocity, V, for p_{air}= 6bar and m_{air}= 752 kg/h . Particles: predictions: O <30μm; Δ 40-50μm; □ 70-80μm; ◊ >90μm

Figure 8 shows typical numerical visualisation of the flow along the axial plane of symmetry, which offer insight into the nature of the flow structure, for all operating conditions, of the droplets spray presents an angle of 45° at exit injector. This figure, still shows a great concentration of droplets, and this is due to the fact that only the larger particles get to reach places nearer the wall duct, and the smaller particles follow closely the flow, as was already previously referenced.

Figure 8a shows that, for RUN 1, the spray impinges on the wall at X/D = 1.54 from the atomiser, which is due to the high initial momentum of droplets as they are injected into duct.

The effect of decreasing the airflow rate at constant pressure of 3 bar is seen by Figures 8a and 8b. This corresponds to a reduction of the air/fuel ratio. The Figure shows that an increase of the fuel-air momentum (achieved in the present case by decreasing the airflow rate at constant air pressure) does not affect the dispersed phase. On the other hand, the Figures 8a and 8c show that the angle of the spray decrease as the ambient pressure increase, for the same mass flow rate of air.

In spite of having included the effect of gravity, which is perpendicular to the main direction of the flow (horizontal), no significant influence is noticed in the flow as can be observed in Figure 8. This picture also confirms the concentration of droplets near the axis of the duct that was already inferred from Figures 6 and 7. It was also observed from Figures 6 and 7 that this effect was associated with the inward movement of the smallest droplets. So, to obtain a better dispersion of the liquid that is decisive to LPP ducts it might be necessary to adopt different types of atomisers and to control the minimum droplet diameter produced.

Conclusions

A computational program was used to study the particle dispersion in polydisperse two-phase turbulent jets, and aims to contribute to a better knowledge of the phenomena occurring inside the premix-prevaporize duct of Low-NOx engines. The previsions were obtained with a commercial full cone (45°) pressure atomiser in an air

flow at pressures up to 6 bar, and the mass flow rate of air varied between 535 kg/h and 752 kg/h. The droplets distribution follow closely to a normal size distribution with a number-average particle diameter of 60μm and a standard deviation of 17μm.

An Eulerian frame for the gas phase was used in conjunction with a Lagrangian approach to describe the effects of both interphase slip and turbulence on particle motion. The computational method yielded good results and revealed great capabilities to improve the knowledge of the particle dispersion phenomena and extend the experimental studies to more complex practical configurations.

The exchange of momentum and turbulence energy between the two phases was shown to play a decisive role on the flow development. The predictions confirmed the measurements and showed that particles follow the turbulence gas flow, affect it significantly. In general, the results quantify the expected trends for a full-cone spray, in that, for a given air pressure and for a given air-liquid flow ratio, larger droplets move outward while smaller droplets move closer to the axis of duct. So, to obtain a better fuel dispersion, which is decisive to LPP, it is necessary to control the minimum droplet diameter produced that may require new types of atomisers.

The previsions show that the angle of the spray decreases as the ambient pressure increases, and an increase of the fuel–air momentum, achieved in the present case by decreasing the air flow rate by 30% at a constant air pressure, does not affect the dispersed phase, but further research is still needed.

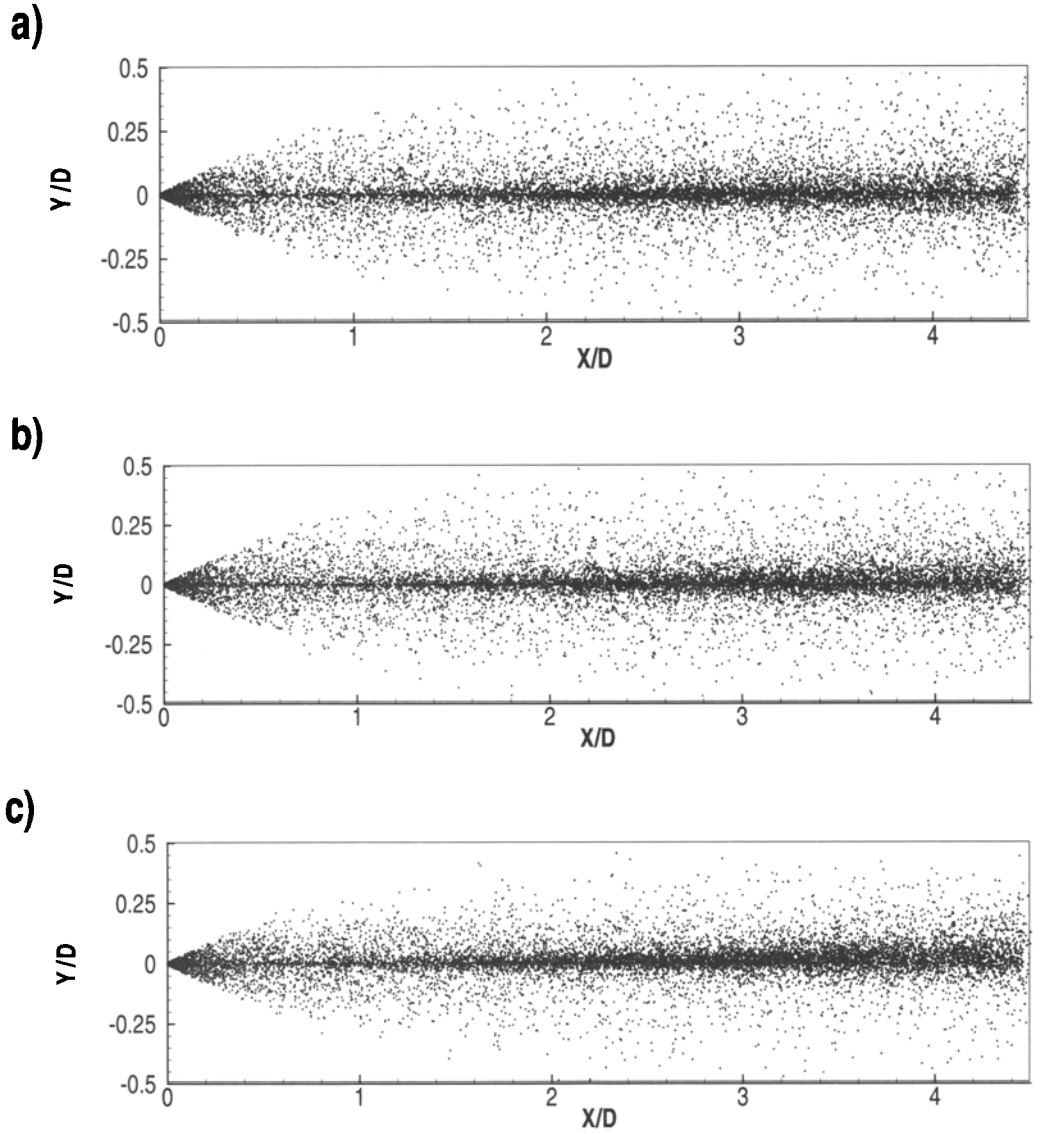

Fig.8 Numerical visualisation of the flow a) 3 bar, m_{air} = 752 kg/h; b) 3 bar, 535 kg/h and c) 6 bar, 752 kg/h

Acknowledgements

The present work has been performed in the scope of the activities of the Aero-Thermodynamics Group for Aerospace Sciences and Technology, and was sponsored by the Portuguese Ministry of Science under Contract Praxis XXI n° CTAE/3/3.1/1917/95 and Grant n° BTI/17135/98.

References

[1] Faeth, G.M., "Evaporation and Combustion of Sprays," Progress Energy Combustion Science, **9**, pp. 1-76, (1983).

[2] Barata, J.M.M., and Perestrelo, N.F.F., "Numerical Simulation of Injection Systems for Lean Burn, Premixed, Prevaporised Combustors," AIAA XIVth International Symposium on Air Breathing Engines, Florence, Italy, 5-12 September, (1999).

[3] Heitor, M.V. and Moreira, A.L.M., "Experiments on Polydisperse Two-Phase Turbulent Jets," ICLASS-94, Rouen, France, Paper XI-5, July (1994).

[4] Barros, A., "Projecto e Construção de um Labotatório de Atomização a Alta Pressão," Tese de Mestrado, Instituto Superior Técnico, Dezembro de, (1997).

[5] Launder, B.E., and Spalding, D. B., "The Numerical of the Turbulent Flows", Computer Methods in Applied Mechanics and Engineering, **3**, pp. 269-289, (1974).

[6] Shirolkar, J.S., Coimbra, C.F.M., and Queiroz McQuay, M., "Fundamentals Aspects of Modeling Turbulent Particle Dispersion in Dilute Flows," Progress. Energy Combustion Science, **22**, pp. 363-399, (1996).

[7] Modaress, D.T., and Elgobashi, S., "Two Component LDA Measurements in a Two-Phase Turbulent Jet," AIAA Journal, **22**, No. 5, pp. 624-630, (1984).

[8] Crowe, C.T., Sharma, M.P. and Stock, D.E., "The Particle Source in Cell (PSI-CELL) Method for Gas-Droplet Flows," Journal Fluid Engineering, **99**, pp. 325-332, (1977).

[9] Patankar, S.V., and Spalding, D.B., "A Calculation Procedure for Heat, Mass and Momentum Transfer in Three-Dimensional Parabolic Flows," International Journal of Heat and Mass Transfer, **15**, pp. 513-527, Oct. (1992).